A Novel Solid Mechanics Approach to Modelling the Interaction of the Left Ventricle and Blood Cavity

Concannon J., McGarry JP.

Biomedical Engineering, College of Engineering and Informatics, University of Galway

Corresponding author: jamie.concannon@universityofgalway.ie

Abstract

This paper presents a novel computationally-efficient physical-based solid/fluid constitutive framework for modelling the cardiac cycle using the finite element method. Previous models of the left ventricle simulate the cardiac cycle by applying pressure or nodal displacements as boundary conditions, which in reality are both ouptuts that are generated due to the interaction between the active contractility of the ventricular myocardium and the temporally varying fluid domain which it encloses. By modelling the blood cavity using C3D8 solid continuum elements, a Windkessel-type volumetric stress formulation governs the pressure-volume relationship during ejection using a central-difference scheme within the user-defined material subroutine. We have developed a patient-specific model of the left ventricle directly from CINE Echocardiography scan data and the model can accurately capture the key trends of Inferior Vena Cava Occlusion (IVCO) experiments, demonstrating the Frank-Starling mechanism as an output. For the first time, the effect of including nonlinear aortic compliance on ventricular pressure-volume loops is studied, and it is demonstrated its inclusion is critical to accurately capture key features of IVCO and endovascular aortic repair (EVAR) experiments. This model acts as an alternative to computationally expensive fluid-structure interaction simulations, and overcomes multiple limitations of current finite element models, and can run full cardiac cycles of a patient-specific left ventricle in 5 minutes, rendering it feasible for clinical integration and real time analysis of patient ventricle dynamics.

Keywords: left ventricle, pressure-volume loop, active contractility, patient-specific, solid/fluid constitutive model

Introduction

Blood pressure in the left ventricle is generated by the interaction of the actively contracting and relaxing myocardial wall with the blood cavity which it encloses. The opening and closing of mitral and aortic valves are controlled by a temporally varying competition between left ventricle pressure, and pulmonary and systemic pressures. This competition in turn alters the boundary conditions experienced by the actively contracting left ventricle. The systemic and pulmonary pressures also vary significantly due to external factors, such as the Windkessel effect or inferior vena cava occlusion (IVCO), rendering the entire heart beat interdependent and complex to model computationally. To simulate the cardiac cycle, the computational biomechanics community rely on either fluid structure interaction (FSI) or finite element analysis (FEA) techniques.

FSI is a multiphysics, bidirectional coupling between the laws that describe fluid dynamics and structural mechanics [1]. Several commercially available software packages exist including; Comsol, Abaqus, Ansys, and FEbio, each of which, through solving the Navier-Stokes equations, are capable of

generating visually impressive particle tracking analyses, streamlines, and moving fluid visualizations. In the context of cardiac modelling however, FSI simulations require complex boundary conditions at the inlets and outlets, and are extremely computationally expensive. Take for example an FSI study by Deng et al., who model the left ventricle wall, bounded fluid domain and mitral valve [2]. The model neglects active contractility of the ventricular myocardium, and the volume versus time plots presented in the results section lack the ability to capture the key features of the widely accepted experimental curves [3]–[8], in particular, the late diastolic plateau evident experimentally before atrial contraction. Another FSI study by Mao et al., modelled the left atrium, ventricle and outflow tract, including the mitral and aortic valves [9]. They too neglect active contractility and prescribe a constant pressure boundary condition at the left atrium, which contradicts the unequivocal experimental evidence that the left atrial pressure varies significantly throughout the cardiac cycle [10]–[16]. Notwithstanding the importance of accurately representing the complex physics of the system in the model, FSI models report cardiac simulation times of 36 hours [17], 90 hours [18], and 168 hours [19], limiting their integration into clinical practice at the moment. Although these complicated simulations can be now run locally, typical runtime being in the order of hours/days [20] is still a limiting factor of the technique.

FEA, (the second approach), is a numerical technique that subdivides the structure of interest into multiple sub-domains, known as elements that are connected to each other via nodes. The FE method formulation of a boundary value problem results in a system of algebraic equations. The simple equations that model the finite elements are then assembled into a larger system of equations that models the entire problem. Currently, there are two main approaches to modelling a cardiac cycle using FEA in the literature; (i) via the application of pressure boundary conditions [21]–[24], and (ii) via the application of displacement boundary conditions [25]–[28] to the myocardial wall to impose a volume change. However, there is a fundamental flaw in both of these approaches, as both pressure and volume should be outputs of the model (and not inputs), as they come from the interaction of the actively contracting ventricular myocardium with the blood volume which it encloses. The pressure-volume (P-V) relationship also depends on the stage of the cardiac cycle, and specifically whether the mitral or aortic valves are open or closed. In FEA models without an actual ventricular blood domain, a constraint equation must be solved during the isovolumetric phase to determine the necessary ventricular pressure to retain the volume of the ventricles. It should be noted however, that the isovolumetric contraction and relaxation sections of a P-V loop are almost never entirely vertical, indicating some volume change [29]–[32]. Once the ventricular pressure exceeds the aortic pressure, the aortic valve will open and the relationship between pressure and volume is often related via a windkessel-type circulatory model.

The problem with current FEA models that attempt to model this windkessel-type circulatory behaviour is that pressure or volume are treated as inputs to these simulations. For example, the endocardium is loaded with a spatially uniform pressure determined by the arterial windkessel pressure, atrial pressure, or volumetric constraint pressure depending on the phase of the cardiac cycle in [33]. Moreover, a spatially uniform pressure is not obtained in the left ventricle according to experimental evidence [34]. Kerkhoffs et al., describes the four major modules required to couple the FE and circulatory model (pressure update, circulatory model, perturbation of circulatory model, and FE model). This iterative approach requires that pressures be updated such that cavity volumes from the FE and circulation models are within a given tolerance, a highly computationally expensive process [35]. Recent studies have used a time-varying elastance model for the ventricle to simulate the full cardiac cycle [36], [37], however this model assumes an exponential end-diastolic P-V relationship and a linear end-systolic P-V relationship, and the P-V relationship for any points between these two is described by a smooth time-varying function [38]. Experimental evidence of P-V loops however, shows a highly non-linear end-systolic P-V relationship [30], [39], [40]. Others have recognised the relationship between pressure, volume, and active stress; Cervantes et al., report an approach whereby for increasing pressures, the active fibre stretch is tuned such that the resulting volume yields a point on the PV loop, however this requires the PV loop to be predefined [41]. Hassaballah et al., modelled the blood cavity using a 9-noded hydrostatic fluid element, with 8 nodes on the internal surface of the left ventricle cavity and a 9^{th} (pressure) node at the centroid of the ventricle base, however a predefined

value of pressure was used which requires the definition of fluid or fluid link elements [42]. The living heart model (LHM) (Dassault Systemes), is an anatomically accurate electro-mechanical model of the entire heart and great vessels, comprised of ~7.5M nodes, and uses surface-based fluid cavity representations of the four heart chambers [43]. The Abaqus surface-based-fluid-cavity feature however, is only available is Abaqus/Explicit, which does not enforce a Newton-Raphson convergence algorithm and requires additional definitions of fluid-exchange and inflator features [44]. Moreover, a single LHM simulation takes 40 hours using 160 CPU cores to solve [45]

In this study we describe a novel approach that addresses all of the abovementioned drawbacks with conventional techniques for simulating a cardiac cycle computationally. We mesh the entire fluid and wall of the left ventricle but don't perform an FSI analysis, we model the fluid using C3D8 solid continuum elements. We develop patient-specific solid/fluid model of the left ventricle directly from CINE Echocardiography scan data using Matlab (Mathworks Inc.), with a user defined constitutive law that governs the pressure and volume of the left ventricle during each of the key phases of the cardiac cycle; (i) isovolumetric contraction, (ii) ejection, (iii) isovolumetric relaxation, and (iv) filling. Our framework allows for the simulation of Inferior Vena Cava Occlusion (IVCO) experiments, the integration of nonlinear aortic compliance, and the simulation of endovascular aortic repair (EVAR) or aortic stenting, on the P-V relationship of the left ventricle. Excellent agreement is observed with experimental studies throughout, and our full patient-specific left ventricle finite element model runs a full cardiac cycle in less than 5 minutes, rendering the approach far more computationally efficient and clinically feasible than previous models to date.

Methodology

In this paper, a solid-fluid left ventricle finite element model is created that can accurately capture the key physics of a cardiac cycle through a PV loop. First, a framework is designed to generate patient specific FE models directly from TriPlanar Echocardiography scan data. A physically based constitutive law for the myocardium is presented, that accounts for the individual contributions of the wall constituents using a constrained mixture approach (ie collagen, cardiomyocytes, groundmatrix). Then a continuum based fluid constitutive model is presented which describes the P-V relationship throughout each phase of the cardiac cycle, as a function of bulk fluid incompressibility during isovolumetric and filling phases and a function of aortic compliance and resistance during ejection.

Multiplanar CINE Echocardiography derived Finite Element Mesh

As part of this study, a MATLAB framework was created for generating patient specific finite element meshes of the left ventricle using multi-planar CINE echocardiography datasets. Capturing images of the left ventricle using 2-Chamber, 3-Chamber and 4-Chamber planes, results in three image datasets each separated by an angular orientation separation of 60º (See **Figure 1(a)**). The frames corresponding to end diastole in each of the datasets is used for mesh generation. The boundary of the inner ventricular wall is defined in each image (**Figure 1(b)**), and rotation of the 2-Chamber and 4-Chamber boundary coordinates by 60º and 120º respectively results in three splines, which meet at the apex and define the three-dimensional internal morphology of the ventricle (**Figure 1(c)**). Regularized resampling of each spline is performed such that each spline contains the same number of points. At each level along the long axis of the ventricle, another spline is then fit to pass through each of these six points (2-red,2-green, 2-blue). The point spacing of these splines defines the mesh density, as each point a node in the initial surface mesh of the finite element model. This surface mesh is then offset outwards to form the wall of the ventricular myocardium using C3D8 solid continuum elements.

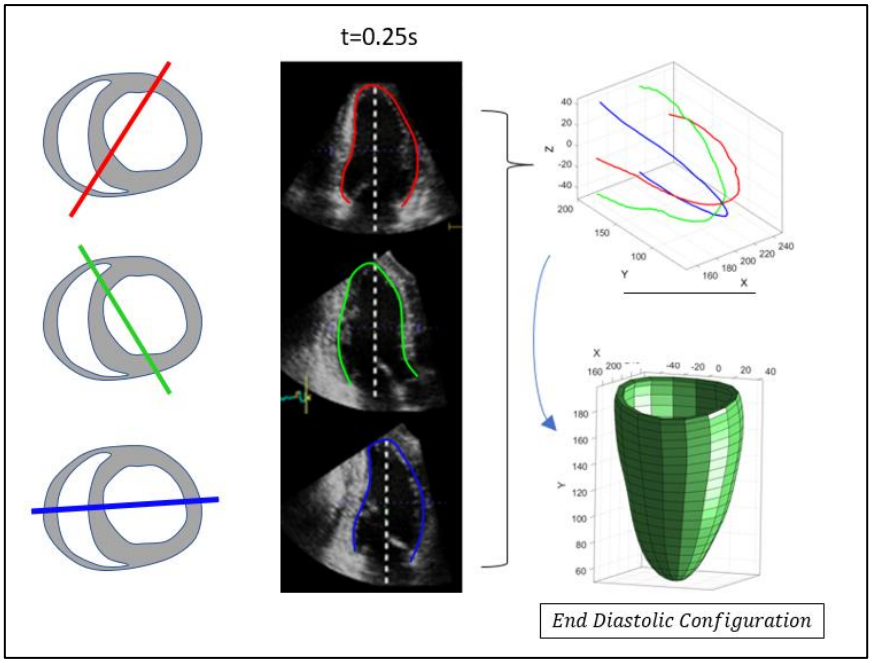

Figure 1: Flowchart of Finite Element Mesh generation from multi-planar echocardiography.

Reference Configuration

If we assume that the reference configuration for the finite element simulation is that of end diastole (MVc in **Figure 2(a)** below), following isovolumetric contraction, ejection, and isovolumetric relaxation, the final filling step would be driven only by the relaxation of the actively contracted cardiomyocytes. However, if we assume that the reference configuration is somewhere below the end diastolic configuration and incorporate the phase of late filling of the ventricle due to atrial contraction as a precursor step to isovolumetric contraction, ejection, and isovolumetric relaxation, the final filling step is now driven by both relaxation of the cardiomyocytes and elastic recoil of the compressed groundmatrix of the ventricular myocardium.

This elastic recoil or restoring forces have been widely reported in the literature. The concept of an equilibrium volume implies that when the end systolic volume is less than the equilibrium volume of the ventricle, the restoring forces will aid in filling [46], or if mitral flow is prevented, will produce a negative pressure [47], [48]. It should be also noted that as the end systolic volume decreases the magnitude of the negative pressure increases. Nikolic et al., found that in 72 of 75 runs in 11 dogs, the equilibrium volume was greater than the end systolic volume, and that diastolic suction was a key feature of the filling phase [49]. Brecher found that when ventricular pressure became negative during mitral valve occlusion, that fluid was aspirated into the heart through a cannula from a reservoir below heart level [50]. Finally, Park et al., point out that if the expansion of the ventricle was a direct result of transmitral flow, these should be in phase with each other. However, they report that for the greater part of the rapid filling phase, left ventricular pressure falls while cavity size increases [51]. This is also observable in the recordings of Fukuta & Little [52]. The abovementioned studies inform our decision in this paper to define the reference volume as ~60% of the end diastolic volume by multiplying the nodes in our finite element mesh by a scalar multiplier, α (**Figure 2(b)**).

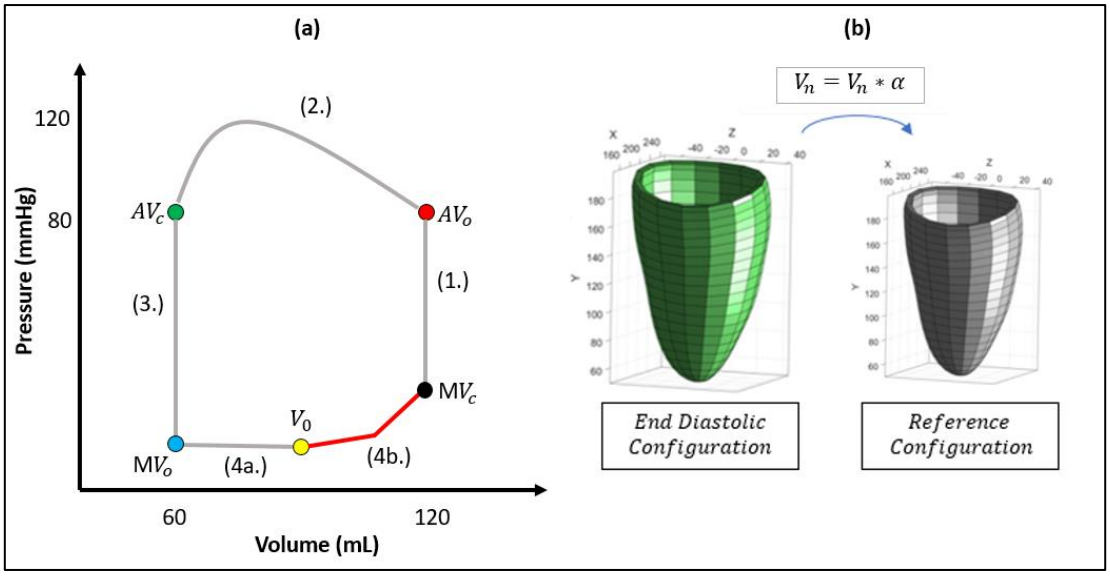

Figure 2: (a) Schematic of PV loop showing phases of the cardiac cycle; (1.) isovolumetric contraction, (2.) ejection, (3.) isovolumetric relaxation, and (4.) filling. AV and MV represent the aortic and mitral valves respectively where subscripts 'o' and 'c' indicate an open or closed position. Each of these phases of the cardiac cycle are described in detail in Section 2.4 The Reference Configuration is depicted as V_0. (b) Scaling of ventricle mesh from end diastolic to reference configuration, where α is the scale factor multiplied by each set of nodal coordinates.

Myocardium Constitutive Law

The constitutive model for the ventricular myocardium employs a rule of mixtures approach where each component of the wall undergoes the same strain, but the stresses are additive, and the sum of constituent densities equals unity [53]. The constituents of the wall explicitly modelled include collagen, elastin, cardiomyocytes, and ground-matrix. A bilinear strain energy function describes the strain stiffening behaviour of fibrillar collagen under tension

$$\boldsymbol{\sigma}_{\text{col}} = V_{col}^{f} * \begin{cases} 0 & \varepsilon < 0 \\ (k_1\varepsilon) * (\boldsymbol{a}_{col} \otimes \boldsymbol{a}_{col}) & 0 \le \varepsilon < \varepsilon_t \\ (k_1\varepsilon + k_2(\varepsilon - \varepsilon_t)) * (\boldsymbol{a}_{col} \otimes \boldsymbol{a}_{col}) & \varepsilon_t \le \varepsilon \end{cases} \quad (1)$$

where V_{col}^{f} is the volume fraction of collagen in the wall, k_1 is the initial stiffness of collagen, k_2 is the secondary stiffness of collagen, ε_t is the transition strain, ε is the strain, and $\boldsymbol{a}_{col}$ denotes the current direction of deformed collagen fibres with respect to the circumferential axis of the artery, where $\boldsymbol{a}_{col} = \mathbf{F}\boldsymbol{a}_{col}^{0}$ (**F**=deformation gradient, and $\boldsymbol{a}_{col}^{0}$ is the direction of undeformed collagen fibres in the reference configuration) [54]. Elastin fibres may also contribute to the anisotropy of the myocardium with a mean directionality defined by $\boldsymbol{a}_{ela}$ such that the stress is

$$\boldsymbol{\sigma}_{ela} = V_{ela}^{f} * \left(\left(\sqrt{I_{4e}} - 1\right) * k_e\right) * (\boldsymbol{a}_{ela} \otimes \boldsymbol{a}_{ela}). \quad (2)$$

I_{4e} is the elastin fibre anisotropic invariant, i.e. the square of stretch of an elastin fibre, ($I_{4e} = (\boldsymbol{a}_{ela} \cdot \mathbf{C}\boldsymbol{a}_{ela})$, where **C** is the right Cauchy-Green Tensor). As described above for collagen, $\boldsymbol{a}_{ela} = \mathbf{F}\boldsymbol{a}_{ela}^{0}$. For anisotropic invariant of the type I_{4k}, we use full invariant rather than the isochoric invariant. This is necessary for reasons outlined in our previous paper [55]. V_{ela}^{f} is the volume fraction of elastin in the wall, and k_e is the stiffness of elastin.

We also incorporate the active component of the wall as represented by σ_{cmy}. The contractile stress generated by a single cardiomyocyte (σ_{act}) is 25 kPa [56]. Cardiomyocytes also contribute to the anisotropy of the vessel through $\boldsymbol{a}_{cmy}$

$$\boldsymbol{\sigma}_{cmy} = V_{cmy}^{f} * \left(\sigma_{act} * \left(\boldsymbol{a}_{cmy} \otimes \boldsymbol{a}_{cmy}\right)\right) \quad (3)$$

where V_{cmy}^{f} is the volume fraction of SMCs in the wall, σ_{act} is the active stress of an individual cardiomyocyte and $\boldsymbol{a}_{cmy} = \mathbf{F}\boldsymbol{a}_{cmy}^{0}$. The active stress versus time waveform is shown in **Figure 3(b)** below. Finally, the stress in the isotropic ground-matrix can be defined as

$$\boldsymbol{\sigma}_{\text{mat}} = V_{mat}^{f} * \begin{cases} E_1(\bar{\lambda}_i - 1) & (\bar{\lambda}_i - 1) \le \varepsilon_{t1} \\ p_m(\bar{\lambda}_i - 1)^2 + q_m(\bar{\lambda}_i - 1) + r_m & \varepsilon_{t1} < (\bar{\lambda}_i - 1) < \varepsilon_{t2} \\ E_2(\bar{\lambda}_i - 1 - \varepsilon_{t2}) + (p_m(\varepsilon_{t2})^2 + q_m(\varepsilon_{t2})^2 + r_m) & (\bar{\lambda}_i - 1) \ge \varepsilon_{t2} \end{cases} \quad (4)$$

where

$$p_m = (E_1 - E_2)/2(\varepsilon_{t1} - \varepsilon_{t2}) \quad (5)$$

$$q_m = E_1 - 2\varepsilon_{t1}p_m \quad (6)$$

$$r_m = (E_1 - q_m)\varepsilon_{t1} - p_m(\varepsilon_{t1})^2 \quad (7)$$

V_{mat}^{f} is the volume fraction of matrix in the wall, E_1 and E_2 are the initial and secondary stiffness of the matrix, ε_{t1} and ε_{t2} are the initial and secondary transition strains. Equations 5-7 must be enforced for continuity. **Figure 3(a)** shows the passive myocardium model simulation for uniaxial tension compared to experimental data, while **Figure 3(b)** details the cardiomyocyte active contractility versus time curve for each phase of the cardiac cycle. The physical parameter values for the passive model are shown in **Figure 3(c)**.

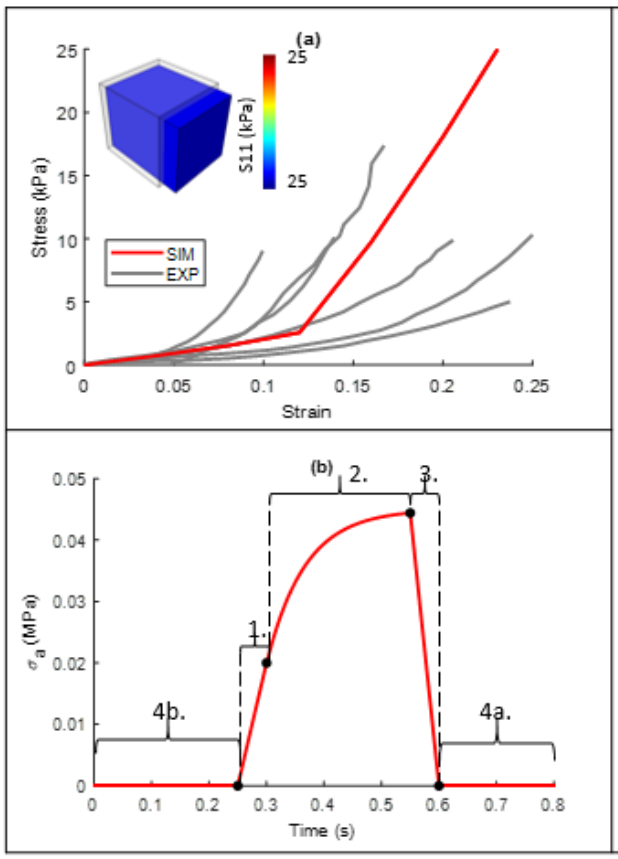

(c)

Parameter	Value
ε_{t1}	0.119
ε_{t2}	0.121
E_1(MPa)	0.0075
E_2(MPa)	0.075
Scale	1.0
κ (MPa)	23.36
k_1(MPa)	0.0025
k_2(MPa)	0.025
θ (°)	150,120,90,60,30
k_e(MPa)	0.000001
ε_{tc}	0.12
V_{col}^{f}	0.3
V_{ela}^{f}	0.2
V_{cel}^{f}	0.3

Figure 3: (a) Simulated (SIM) vs experimental (EXP) passive myocardium stress-strain data for uniaxial tension, using the myocardium constitutive law described above. (b) The active stress (σ_{act}) versus time profile for each phase of the cardiac cycle; (1.) isovolumetric contaction, (2.) ejection, (3.) isovolumetric relaxation, (4a.) early filling, and (4b.) late filling. (c) The parameters and values of the constitutive law corresponding to the stress-strain response shown in (a).

Fluid Constitutive Law

Consideration of the interaction between the ventricular myocardium and the internal blood is a key feature of this model. Fundamentally, by neglecting the fluid and allowing the ventricle to contract against an empty cavity will result in an underestimation of the level of active contractility required to reach the end systolic configuration. In this study the fluid volume is meshed with C3D8 solid continuum elements where the outermost fluid element layer share nodes with the innermost layer of the myocardium. We tie these nodes in order to simulate contact between the wall and the blood. The physics of the blood changes in each stage of the cardiac cycle depending on the opening and closing of the aortic and mitral valves. The detail of such is described below according to each stage. In each stage the shear modulus of the blood is negligible compared to the volumetric.

Step 4b (Late Filling):

In late diastole, the left atrium contracts while the mitral valve is opened, resulting in an increase in system pressure and ventricular volume. This pressure increase in the ventricle due to atrial contraction is modelled by applying a outwards pressure on the inner myocardium wall of 15mmHg, which expands the fluid domain outwards also (the interface nodes are shared between the blood and the wall). We allow the fluid to deform freely with a low bulk modulus (κ=1.0e-08 MPa) according to

$$\sigma_h = \kappa(J-1)J \tag{8}$$

Where J is the Jacobian (determinant of the deformation gradient tensor). We then employ a pressure transfer equilibrium step, whereby we remove the pressure boundary condition from the wall, and increase the bulk modulus to κ=1 MPa, which results in the wall generating an internal fluid stress of 15mmHg as desired. This step ends at the onset of active contractility. Throughout the rest of this study we denote ($\kappa^{\Uparrow} = 1.0\ MPa$) and ($\kappa^{\Downarrow} = 1.0e-08\ MPa$).

Step 1 (Isovolumetric Contraction):

During isovolumetric contraction both the mitral valve and the aortic valve are closed. The active contractility of the myocardium increases and acts against the incompressible fluid volume which it encloses. We model this by using the simple volumetric formulation

$$\sigma_h = \kappa^{\Uparrow}(J-1)J \tag{9}$$

As the ventricle contracts against the high bulk modulus fluid, pressure is generated in the fluid with negligible volumetric deformation of the elements, and we observe the characteristic right vertical line of the PV loop. This stage ends when the ventricular pressure exceeds the aortic pressure.

Step 2 (Ejection):

Once the ventricular fluid pressure exceeds that of the aortic pressure, the aortic valve opens and blood is ejected into the systemic circulation. The physics of the blood in this step is captured using a Windkessel formulation that relates the pressure to the flow

$$P = P_t + \left(\frac{-RFdV_e - P_t dt}{RC + 0.5dt}\right) \tag{10}$$

$$\sigma_h = -P \tag{11}$$

where P_t is the previous pressure, R is the aortic resistance (), C is the aortic compliance (1.0 cm^3/mmHg), F is a scale factor mapping element to ventricle volume ($F = V_{vo}/V_{eo}$), dV_e is the incremental change in volume of the element ($dV_e = J(V_{en} - V_{ep})$), and dt is the time increment. This stage ends when the ejection time has passed (0.25s).

Step 3 (Isovolumetric Relaxation):

During isovolumetric relaxation, again, both the mitral valve and the aortic valve are closed. The active contractility of the myocardium this time decreases rapidly and attempts to expand the incompressible fluid volume which it encloses. We model this stage also by using the simple volumetric formulation

$$\sigma_h = \kappa^{\Uparrow}(J-1)J \tag{12}$$

Step 4a (Early Filling):

Once the pressure in the ventricle drops below the pulmonary pressure, the mitral valve opens and blood can enter the ventricle. We model this stage also by using the simple volumetric formulation

$$\sigma_h = \kappa^{\Downarrow}(J-1)J \tag{13}$$

If we assume that by the end of the isovolumetric relaxation phase, the active contractility is fully removed ($\sigma_{act} = 0$), then the expansion of the ventricle in this step is driven primarily by the restoring forces of the ventricle (the compression springback of the groundmatrix which has been compressed below its reference configuration by the active contractility in Step 3). With a low bulk modulus of the fluid, the relaxation of the myocardium to the reference configuration results in a fluid expansion with negligible pressure increase. Alternatively, if we assume that by the end of the isovolumetric relaxation phase, the active contractility is *not* fully removed ($\sigma_{act} > 0$), then the expansion of the ventricle in this step is driven by a combination of the restoring forces and the relaxing residual active contractility.

Results

Paramteric Analysis

As described in the previous section, our model is physically based, allowing for a physiologically based calibration of the model rather than a black-box fitting of parameters. As a consequence the only unknown in the model is the σ_a versus time profile. In order for the PV loops to behave according to experiments, we know that σ_a must increase during isovolumetric contraction, continue to increase at a reduced slope in ejection, and then decrease rapidly during isovolumetric relacation until the mitral valve opens at such a point we enter the filling stage. **Figure 4** shows the influence of active stress magnitude and rate of contractility build-up on the PV loops, in addition to the influence of aortic compliance (C) and peripheral resistance (R) in a parametric analysis. It is observed that decreasing C, or equivalently increasing aortic stiffness results in a reduced stroke volume and increased peak left ventricular pressure (**Figure 4: Row 1**). Increasing R results in a significant reduction in stroke volume with little effect on peak pressure (**Figure 4: Row 2**). Increasing the magnitude of σ_a increases stroke volume, and peak left ventricular pressure (**Figure 4: Row 3**). Finally the rate of contractility build-up alters the shape of the PV loop only in the ejection phase (**Figure 4: Row 4**).

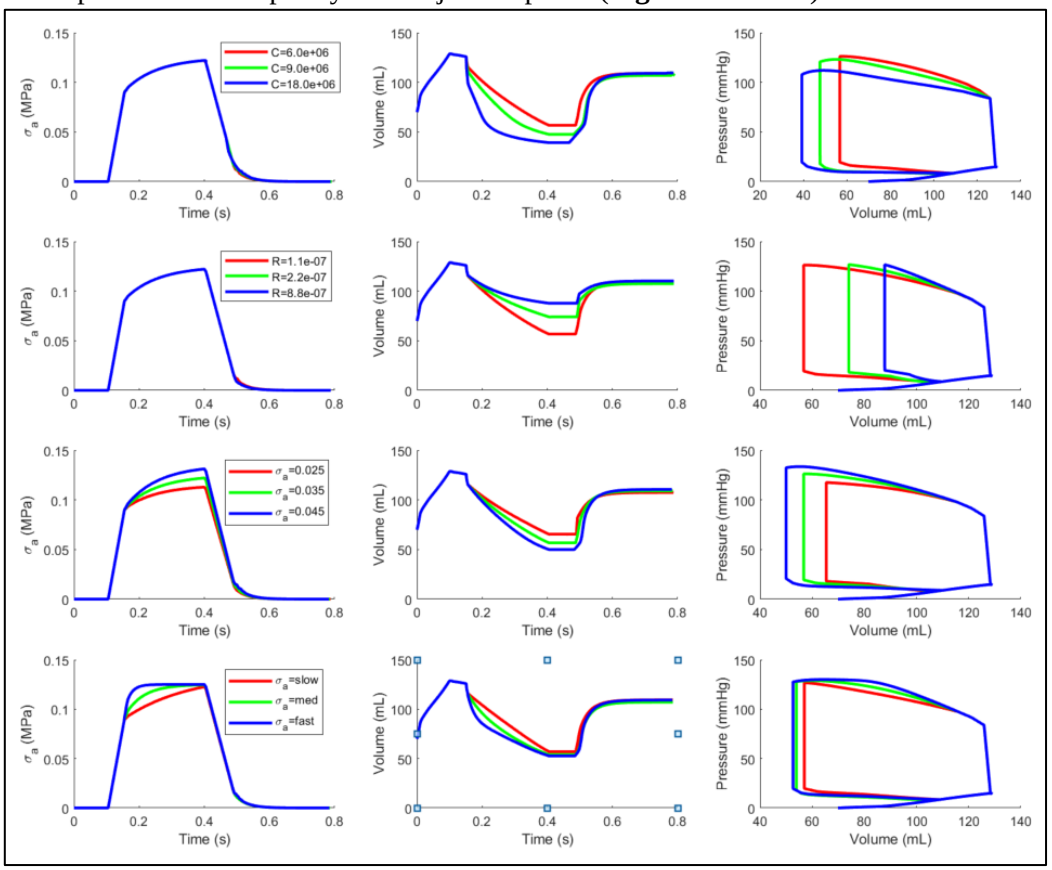

Figure 4: (a) Parametric analysis on Compliance, Resistance, active stress magnitude and rate. Unless otherwise stated parameters follow those in Figure 3(c).

Inferior Vena Cava Occlusion (IVCO)

IVCO is commonly performed to measure baseline contractility clinically [57]–[59]. Occluding the IVC reduces venous return to the right atrium which results in a decreased left atrium pressure in subsequent cardiac cycles. 4 key features are evident from the IVCO experiments; (i) a reduction in aortic valve opening pressure (ii) a reduction in aortic valve closing pressure, (iii) a reduction in stroke volume, and (iv) a change in ejection slope from bilinear at the beginning to linear at the end of the IVCO experiment. **Figure 5** shows the experimental PV loop adapted from Pinsky et al., 2018 (Exp), with our model simulation (Sim) superimposed. Our computational model prediction for IVCO captures the first 3 of the 4 features described above with a *linear Compliance* (C).

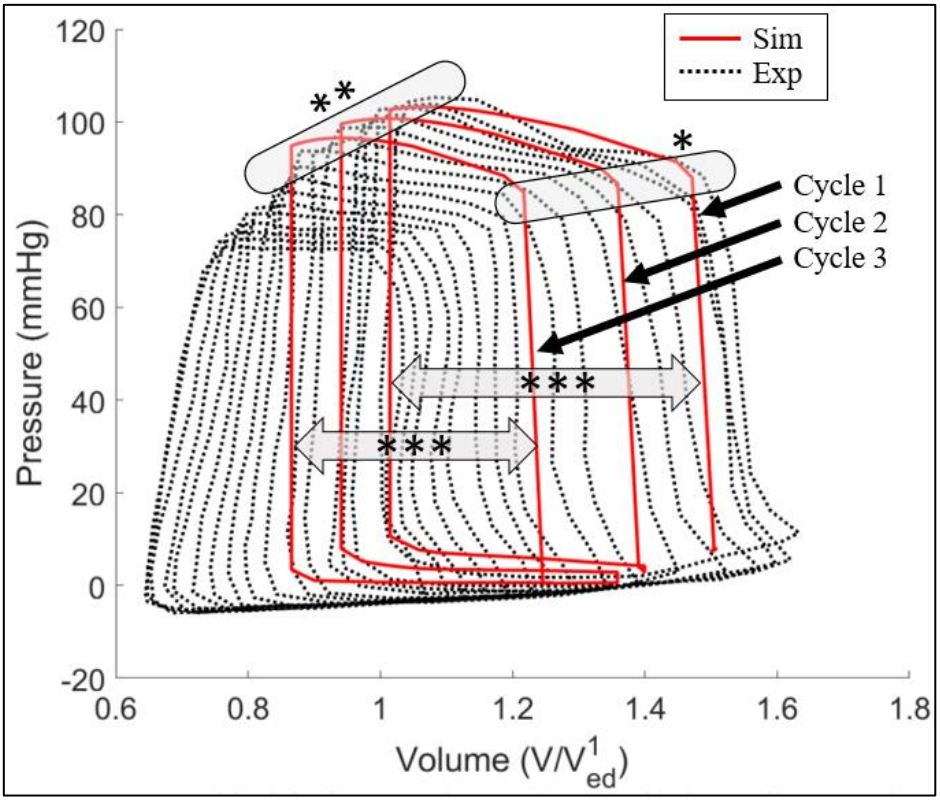

Figure 5: Simulation (Sim) compared to Experimental study (Exp) of Garcia & Pinsky (2018) [30]. Simulated: Our model captures the first 3 of the 4 key experimental features; (i) reduction in aortic valve opening pressure (*); (ii) reduction in aortic valve closing pressure (**), and (iii) reducting stroke volume (***) with every additional cardiac cycle using linear compliance.

Nonlinear Aortic Compliance

Evidence exists that the aorta exhibits a nonlinear compliance both *ex-vivo* and *in-vivo* within each cardiac cycle, with a high compliance at low pressures and a low compliance at high pressures [60]–[63]. **Figure 6** below shows the effect of integrating nonlinear aortic compliance on the ventricular PV loop when compared to the linear compliance model shown in **Figure 5**. In order to capture the fourth feature of the IVCO experiments ((iv) a change in ejection slope from bilinear at the beginning to linear at the end of the IVCO experiment), finite element models of the left ventricle, and specifically the constitutive law must include a nonlinear compliance term for the aorta.

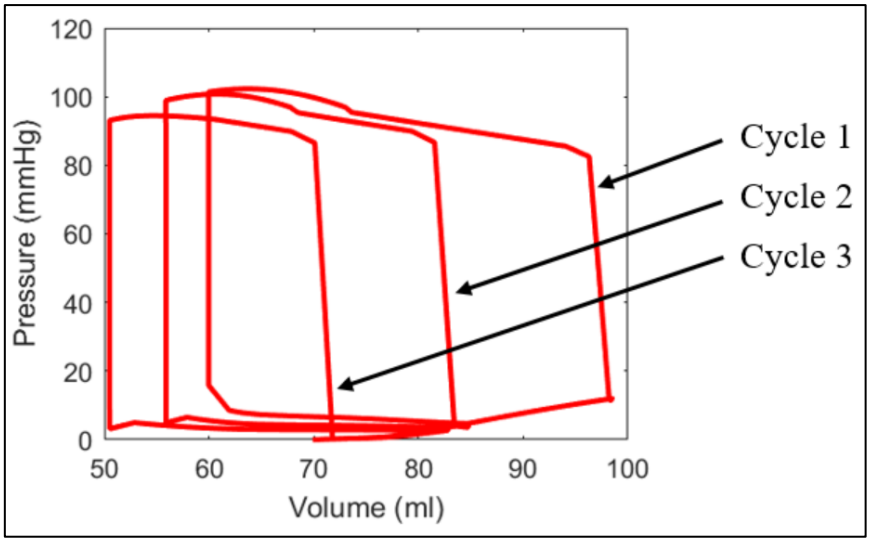

Figure 6: Incorporation of the nonlinear aortic compliance term allows the model to capture the fourth feature of the experimental curves (See Figure 5 (Exp) [30]) ; a change in ejection slope from bilinear at the beginning to linear at the end of the IVCO experiment.

Endovascular Aortic Repair (EVAR)

A recent study by Concannon et al., revealed that aortic stenting expands the aorta beyond the transition strain that separates low from high compliance regimes [64]. The outward force of the stent pushes the aorta into the low compliance regime and equilibrates with the compressive forces of the wall at a new equilibrium configuration such that in all subsequent cycles, the pressure area curve follows that of the low compliance slope. In this study, we model this EVAR computationally by removing the high compliance regime from the nonlinear compliance model (as occurs following stenting). We observe the following trends on the ventricular PV loop: (i) the stroke volume decreases, (ii) peak systolic pressure increases, and (iii) aortic valve opening pressure reduces (diastolic decay reduces). These features can be observed in **Figure 7** where control represents the healthy aorta preoperatively with a nonlinear shaped PV relationship during ejecton, while EVAR represents the stented aorta postoperatively.

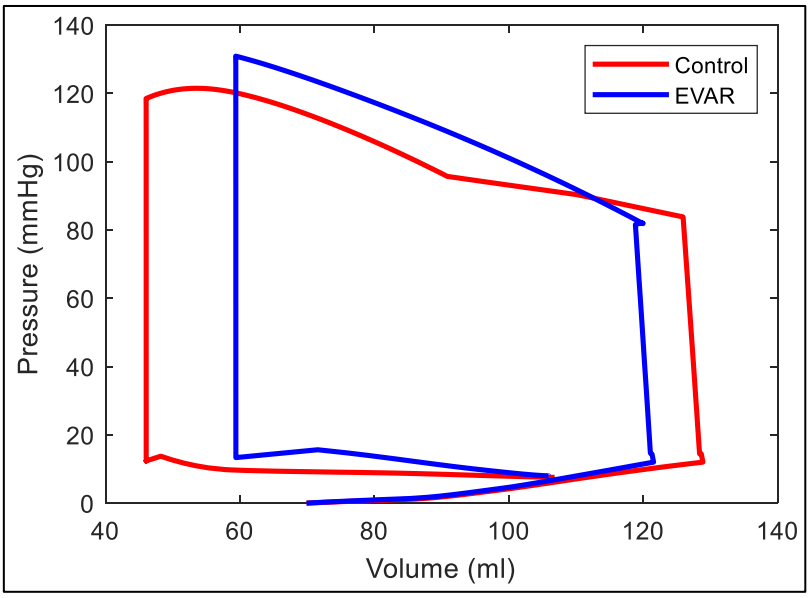

Figure 7: Simulation of the effect of aortic stenting (EVAR) on left ventricular PV loop. In the control case we observe healthy nonlinear PV relationship during ejection, however this is lost postoperstively as the slope follows the low-compliance regime slope resulting in increased systolic pressure, reduced stroke volume and reduced aortic valve opening pressure or increased diastolic decay.

Discussion

In this study we describe a novel approach that surpasses conventional techniques for simulating a cardiac cycle. We mesh the entire fluid and wall of the left ventricle and model the fluid using C3D8 solid continuum elements. We develop a patient-specific solid/fluid model of the left ventricle directly from CINE Echocardiography scan data using Matlab (Mathworks Inc.) with a physically based user defined material subroutine or constitutive law that governs the pressure and volume of the left ventricle during each of the key phases of the cardiac cycle; (i) isovolumetric contraction, (ii) ejection, (iii) isovolumetric relaxation, and (iv) filling. Crucially, this physically-based solid/fluid umat approach predicts the key features of experimental PV loops with pressure and volume as outputs of the model and not inputs as studies to date have incorrectly assumed. Our framework allows for the simulation of IVCO experiments, the integration of nonlinear aortic compliance, and the simulation of EVAR (aortic stenting) on the P-V relationship of the left ventricle. Excellent agreement is seen with experiments throughout, with each cardiac cycle exhibiting a run time of 5 minutes, rendering the approach computationally far more efficient and clinically feasible than current methods.

Physical based prediction of P-V loop

As shown in Figure 4, the parametric study highlights the physical nature of the interaction of the solid/fluid umats in generating P-V loops that capture the key trents observed experimentally. Increasing aortic compliance results in a larger stroke volume, and reduced peak ventricular pressure, as would be expected when the ventricle is pumping blood into a more compliant outflow tract. Decreasing compliance, on the other hand, results in a reduction in stroke volume and an increase in peak systolic ventricular pressure as the active contractility in the myocardial wall is acting against a more rigid conduit. This has also been observed experimentally by Ioannou and colleagues who subjected porcine aortae to banding to decrease vessel compliance which lead to a 41% increase in peak systolic pressure [65]. Parametric analysis on the peripheral resistance term (R) showed little change on peak systolic pressure but significant increase in stroke volume with decreasing R. This has also been observed clinically where a reduction in systemic vascular resistance as patients moved from rest to exercise resulted in an increase in cardiac output [66]. An increase in the magnitude of the active contractility term (σ_a) results in an increased stroke volume, which has been observed in drug infusion studies where dobutamine (positive inotropic agent) resulted in a lower end-systolic volume and verapamil (calcium channel blocker) resulted in a higher end-systolic volume [67].

Modelling IVCO Experiments

The key physics of the cardiopulmonary system emebedded in this model allows for accurate simulation of IVCO experiments, and proves the robustness of the framework to deal with transient reductions in inflow boundary conditions which result from restricting the inferior vena cava. This results in a reduction in left atrial filling pressure which results in drop in aortic valve opening pressure, closing pressure and stroke volume experimentally. Our linear compliance model can capture each of these key features, in contrast to previous models which for example, prescribed the volume in an airbag to model the left ventricle and the end systolic volume does not shift to the left [68] as in experimental studies of IVCO [30], [69]. The reduction in stroke volume that occurs as a consequence of a reduced left ventricle filling pressure during IVCO is an important output of the model and highlights its ability to capture the Frank-Starling mechanism [70] *in-silico*.

Effect of Nonlinear Aortic Compliance on PV loop

Each of the key features of the IVCO experiments bar one can be captured by the linear compliance model described above. Evidence exists however, that the aorta exhibits nonlinear compliance *in-vivo* within each cardiac cycle [63]. Integration of this nonlinear compliance of the aorta in the user defined material subroutine results in a slope change during ejection commensurate with the transition pressure or strain whereby the collagen fibres begin to affect the overall modulus of the vessel wall [53], [71], [72]. Once the aortic valve opens, the left ventricle and aorta become a unified conduit and exhibit the same system pressure, while the overall aortic compliance affecting the ventricle outflow is dependent on the presssure in the aorta, where compliance is now a nonlinear function of pressure. Integration of

this key feature in the model allows for prediction of the experimental shape change seen clinically [30], [69]. This phenomenon can be explained as the transient reduction in left atrial filling pressure as a consequence of occlusion of the inferior vena cava results in the left ventricle opening the aortic valve at a lower pressure each sysle, and the pressure during ejection no longer passes the transition pressure leading to a slope change, or essentially, the aorta no longer enters the low compliance regime.

Simulation of Endovascular Aortic Repair (EVAR)

The current framework readily allows for simulation of the effects of endovacular aortic repair or stenting on left ventricular performance. This is particulary relevant clinically, with recent studies uncovering a link between proximal aortic stenting and left ventricular hypertophy [73], [74] and cardiac deaths [75]. Moreover animal studies have shown that placing a graft in the native porcine aorta diminishes the windkessel effect [76], as evident in this model when the high-compliance regime is removed. In a previous study the authors reported the mechanism by which stenting (EVAR) alters vessel constitutive behaviour [64]. The outward radial force of the stent stretches artery beyond transition strain to a new equilibrium configuration and as such the vessel no longer exhibits a high compliance regime at low pressures, and operates only in the low compliance regime, given the dacron enforced limit is not reached. Simulation of this required removal of the high compliance regime from the constitutive law such that the windkessel formulation only sees the high stiffness throughout the entire cardiac cycle. This results in a reduction in stroke volume and an increase in systolic pressure and reduction in diastolic pressure. This has been shown in both experimental [77], [78] and clinical [79]–[81] studies to date. Takaseya et al., reported that EVAR in 15 aortic aneurysm patients resulted in an increase in systolic blood pressure from 90.4 to 100.4mmHg ($p<0.05$) [82], while Kelly et al., observed an increase in systolc pressure from 110-162mmHg and decrease in diastolic pressure from 76-63mmHg following dacron graft insertion in dogs [83]. Sarraf et al., also observed a reduction in end diastolic pressure following transcatheter aortic valve implantation [84], which acts the same as a stent-graft in altering the mechanical behaviour of the vessel wall through expansion, suggesting this left ventricular response to device-artery compliance mismatch may not be unique to EVAR.

Conclusion

In conclusion, this study has developed a novel computationally-efficient physical based solid/fluid constitutive framework for modelling the cardiac cycle using the finite element method. We have developed a patient-specific model of the left ventricle directly from CINE Echocardiography scan data using Matlab with a user defined constitutive law that governs the pressure and volume of the left ventricle during each of the key phases of the cardiac cycle predicting the PV loop as a result of the interaction between the active contractility of the ventricular myocardium and the fluid domain. The active anisotropic hyperelastic model includes nonlinear aortic compliance and is capable of simulating complex experiments such as IVCO and EVAR in clinically feasible timeframes.

References

[1] "Comsol: multiphysics / fluid structure interaction," 2017. https://www.comsol.com/multiphysics/fluid-structure-interaction.

[2] L. Deng, X. Huang, C. Yang, Y. Song, and D. Tang, "Patient-specific CT-based 3D Passive FSI model for left ventricle in hypertrophic obstructive cardiomyopathy," *Comput. Methods Biomech. Biomed. Engin.*, vol. 21, no. 3, p. 255, Feb. 2018, doi: 10.1080/10255842.2018.1443215.

[3] J. A. Shar, S. G. Keswani, K. J. Grande-Allen, and P. Sucosky, "Significance of aortoseptal angle anomalies to left ventricular hemodynamics and subaortic stenosis: A numerical study," *Comput. Biol. Med.*, vol. 146, Jul. 2022, doi: 10.1016/J.COMPBIOMED.2022.105613.

[4] V. Ferreira Ribeiro, D. C. Leandro De Oliveira, D. Gama Das Neves, N. Simão, V. Nunes, H. V. Junior, and M. S. Nacif, "Cardiac Magnetic Resonance and amyloidosis: Review," *Int. J. Cardiovasc. Sci.*, vol. 32, no. 2, pp. 177–189, 2019, doi: 10.5935/2359-4802.20190005.

[5] L. Sugeng, V. Mor-Avi, L. Weinert, J. Niel, C. Ebner, R. Steringer-Mascherbauer, F. Schmidt, C. Galuschky, G. Schummers, R. M. Lang, and H. J. Nesser, "Quantitative Assessment of Left Ventricular Size and Function," *Circulation*, vol. 114, no. 7, pp. 654–661, Aug. 2006, doi:

10.1161/CIRCULATIONAHA.106.626143.

[6] H. yan Xu, Z. gang Yang, Y. kun Guo, K. Shi, X. Liu, Q. Zhang, L. Jiang, and L. jun Xie, "Volume-time curve of cardiac magnetic resonance assessed left ventricular dysfunction in coronary artery disease patients with type 2 diabetes mellitus," *BMC Cardiovasc. Disord.*, vol. 17, no. 1, pp. 1–9, Jun. 2017, doi: 10.1186/S12872-017-0583-5/FIGURES/4.

[7] S. Hellwig, U. Grittner, M. Elgeti, S. Wyschkon, S. N. Nagel, J. B. Fiebach, T. Krause, J. Herm, J. F. Scheitz, M. Endres, C. H. Nolte, K. G. Haeusler, and T. Elgeti, "Evaluation of left ventricular function in patients with acute ischaemic stroke using cine cardiovascular magnetic resonance imaging," *ESC Hear. Fail.*, vol. 7, no. 5, pp. 2572–2580, Oct. 2020, doi: 10.1002/EHF2.12833.

[8] M. Yang, V. DeMarco, J. Sowers, and L. Ma, "High Temporal Resolution Cine MRI for Early Detection of Left Ventricular Diastolic Dysfunction of the Diabetic Heart," 2011, [Online]. Available: https://wmis.org/abstracts/2011/data/papers/P419.html.

[9] W. Mao, A. Caballero, R. Mckay, C. Primiano, and W. Sun, "Fully-coupled fluid-structure interaction simulation of the aortic and mitral valves in a realistic 3D left ventricle model," 2017, doi: 10.1371/journal.pone.0184729.

[10] M. Gori, A. Iacovoni, and M. Senni, "Haemodynamics of Heart Failure With Preserved Ejection Fraction: A Clinical Perspective," *Card. Fail. Rev.*, 2016, doi: 10.15420/CFR.2016:17:2.

[11] J. Ritzema, I. C. Melton, A. M. Richards, I. G. Crozier, C. Frampton, R. N. Doughty, J. Whiting, S. Kar, N. Eigler, H. Krum, W. T. Abraham, and R. W. Troughton, "Direct Left Atrial Pressure Monitoring in Ambulatory Heart Failure Patients," *Circulation*, vol. 116, no. 25, pp. 2952–2959, Dec. 2007, doi: 10.1161/CIRCULATIONAHA.107.702191.

[12] M. Meyer, S. Bell, N. Sardana, R. Zubarik, M. LeWinter, and H. Dauerman, "Esophageal assessments of left ventricular filling pressures: A proof-of-concept study," *Int. J. Crit. Illn. Inj. Sci.*, vol. 4, no. 1, p. 18, 2014, doi: 10.4103/2229-5151.128008.

[13] K. E. Schober, J. D. Bonagura, B. A. Scansen, J. A. Stern, and N. M. Ponzio, "Estimation of left ventricular filling pressure by use of Doppler echocardiography in healthy anesthetized dogs subjected to acute volume loading," *J. Am. Vet. Med. Assoc.*, vol. 233, no. 4, pp. 617–617, Aug. 2008, doi: 10.2460/JAVMA.233.4.617.

[14] S. F. Nagueh, C. P. Appleton, T. C. Gillebert, P. N. Marino, J. K. Oh, O. A. Smiseth, A. D. Waggoner, F. A. Flachskampf, P. A. Pellikka, and A. Evangelisa, "Recommendations for the evaluation of left ventricular diastolic function by echocardiography," *Eur. J. Echocardiogr.*, vol. 10, no. 2, pp. 165–193, 2009, doi: 10.1093/EJECHOCARD/JEP007.

[15] H. Fukuta and W. C. Little, "Diastolic versus systolic heart failure," *Diastolic Hear. Fail.*, pp. 119–133, 2008, doi: 10.1007/978-1-84628-891-3_8.

[16] A. G. MORROW, E. BRAUNWALD, J. A. HALLER, and E. H. SHARP, "Left Atrial Pressure Pulse in Mitral Valve Disease: A Correlation of Pressures Obtained by Transbronchial Puncture with the Valvular Lesion," *undefined*, vol. 16, no. 3, pp. 399–405, Sep. 1957, doi: 10.1161/01.CIR.16.3.399.

[17] F. Xu, S. Morganti, R. Zakerzadeh, D. Kamensky, F. Auricchio, A. Reali, T. J. R. Hughes, M. S. Sacks, and M.-C. Hsu, "A framework for designing patient-specific bioprosthetic heart valves using immersogeometric fluid-structure interaction analysis," 2017, doi: 10.1002/cnm.2938.

[18] A. Zingaro, I. Fumagalli, L. Dede, M. Fedele, P. C. Africa, A. F. Corno, and A. Quarteroni, "A geometric multiscale model for the numerical simulation of blood flow in the human left heart," *Discret. Contin. Dyn. Syst. - S. 2022, Vol. 15, Pages 2391-2427*, vol. 15, no. 8, p. 2391, Mar. 2022, doi: 10.3934/DCDSS.2022052.

[19] W. W. Chen, H. Gao, X. Y. Luo, and N. A. Hill, "Study of cardiovascular function using a coupled left ventricle and systemic circulation model," *J. Biomech.*, vol. 49, no. 12, pp. 2445–2454, Aug. 2016, doi: 10.1016/J.JBIOMECH.2016.03.009.

[20] M. Toma, S. Singh-Gryzbon, E. Frankini, Z. Wei, and A. P. Yoganathan, "Clinical Impact of Computational Heart Valve Models," *Materials (Basel).*, vol. 15, no. 3302, 2022, doi: 10.3390/ma15093302.

[21] S. M. H. Haddad and A. Samani, "A computational model of the left ventricle biomechanics using a composite material approach," *Int. J. Eng. Sci.*, vol. 111, pp. 61–73, Feb. 2017, doi: 10.1016/J.IJENGSCI.2016.11.008.

[22] F. Dorri, P. F. Niederer, and P. P. Lunkenheimer, “A finite element model of the human left ventricular systole,” *http://dx.doi.org/10.1080/10255840600960546*, vol. 9, no. 5, pp. 319–341, 2007, doi: 10.1080/10255840600960546.

[23] S. Land *et al.*, “Verification of cardiac mechanics software: benchmark problems and solutions for testing active and passive material behaviour,” *Proc. R. Soc.*, vol. 471, no. 2184, 2015, doi: 10.1098/rspa.2015.0641.

[24] J. I. Han, M. Kubala, E. I. Aranda-Michel, and D. R. Trumble, “Ventricle-specific epicardial pressures as a means to optimize direct cardiac compression for circulatory support: A pilot study,” 2019, doi: 10.1371/journal.pone.0219162.

[25] E. McEvoy, W. Wijns, and P. McGarry, “A thermodynamic transient cross-bridge model for prediction of contractility and remodelling of the ventricle,” *J. Mech. Behav. Biomed. Mater.*, vol. 113, p. 104074, Jan. 2021, doi: 10.1016/j.jmbbm.2020.104074.

[26] A. I. Veress, W. P. Segars, B. M. W. Tsui, and G. T. Gullberg, “Incorporation of a Left Ventricle Finite Element Model Defining Infarction Into the XCAT Imaging Phantom,” *IEEE Trans. Med. Imaging*, vol. 30, no. 4, p. 915, Apr. 2011, doi: 10.1109/TMI.2010.2089801.

[27] S. Khodaei, N. Fatouraee, and M. Nabaei, “Numerical simulation of mitral valve prolapse considering the effect of left ventricle,” *Math. Biosci.*, vol. 285, pp. 75–80, Mar. 2017, doi: 10.1016/J.MBS.2016.12.008.

[28] M. H. Moosavi, N. Fatouraee, H. Katoozian, A. Pashaei, and A. F. Frangi, “Using atlas of heart shapes for simulation of blood flow in left ventricle,” *Biomed. Eng. - Appl. Basis Commun.*, vol. 25, no. 6, Dec. 2013, doi: 10.4015/S1016237213500506.

[29] P. H. Pak, W. L. Maughan, K. L. Baughman, and D. A. Kass, “Marked Discordance Between Dynamic and Passive Diastolic Pressure-Volume Relations in Idiopathic Hypertrophic Cardiomyopathy,” *Circulation*, vol. 94, no. 1, pp. 52–60, Jul. 1996, doi: 10.1161/01.CIR.94.1.52.

[30] M. I. Monge Garcia, Z. Jian, J. J. Settels, C. Hunley, M. Cecconi, F. Hatib, and M. R. Pinsky, “Performance comparison of ventricular and arterial dP/dtmax for assessing left ventricular systolic function during different experimental loading and contractile conditions,” *Crit. Care*, vol. 22, no. 1, pp. 1–12, Nov. 2018, doi: 10.1186/S13054-018-2260-1/TABLES/4.

[31] H. Senzaki, C. H. Chen, and D. A. Kass, “Single-Beat Estimation of End-Systolic Pressure-Volume Relation in Humans,” *Circulation*, vol. 94, no. 10, pp. 2497–2506, Nov. 1996, doi: 10.1161/01.CIR.94.10.2497.

[32] A. Ochagavía, L. Zapata, A. Carrillo, A. Rodríguez, M. Guerrero, and J. M. Ayuela, “Evaluation of contractility and postloading in the intensive care unit,” *Med. Intensiva (English Ed.*, vol. 36, no. 5, pp. 365–374, Jun. 2012, doi: 10.1016/J.MEDINE.2012.07.007.

[33] A. A. Bakir, A. Al Abed, N. H. Lovell, and S. Dokos, “Multiphysics Computational Modelling of the Cardiac Ventricles,” *IEEE Rev. Biomed. Eng.*, vol. 15, pp. 309–324, 2022, doi: 10.1109/RBME.2021.3093042.

[34] H. M. El-Husseiny, E. A. Mady, D. Ma, L. Hamabe, K. Takahashi, and R. Tanaka, “Intraventricular pressure gradient: A novel tool to assess the post-infarction chronic congestive heart failure,” *Front. Cardiovasc. Med.*, vol. 9, p. 2220, Aug. 2022, doi: 10.3389/FCVM.2022.944171/BIBTEX.

[35] R. C. P. Kerckhoffs, M. L. Neal, Q. Gu, J. B. Bassingthwaighte, J. H. Omens, A. D. Mcculloch, A. Biomed, and E. Author, “Coupling of a 3D Finite Element Model of Cardiac Ventricular Mechanics to Lumped Systems Models of the Systemic and Pulmonic Circulation NIH Public Access Author Manuscript,” *Ann Biomed Eng*, vol. 35, no. 1, pp. 1–18, 2007, doi: 10.1007/s10439-006-9212-7.

[36] A. C. Estrada, K. Yoshida, J. J. Saucerman, and J. W. Holmes, “A multiscale model of cardiac concentric hypertrophy incorporating both mechanical and hormonal drivers of growth,” *Biomech. Model. Mechanobiol.*, vol. 20, no. 1, pp. 293–307, Feb. 2021, doi: 10.1007/S10237-020-01385-6.

[37] C. M. Witzenburg and J. W. Holmes, “Predicting the time course of ventricular dilation and thickeningusing a rapid compartmental model,” *J. Cardiovasc. Transl. Res.*, vol. 11, no. 2, p. 109, Mar. 2018, doi: 10.1007/S12265-018-9793-1.

[38] H. Sharifi, C. K. Mann, A. L. Rockward, M. Mehri, J. Mojumder, L. C. Lee, K. S. Campbell,

and J. F. Wenk, “Multiscale simulations of left ventricular growth and remodeling,” *Biophys. Rev. 2021 135*, vol. 13, no. 5, pp. 729–746, Aug. 2021, doi: 10.1007/S12551-021-00826-5.
[39] S. Yar, M. M. Monasky, and R. J. Solaro, “Maladaptive modifications in myofilament proteins and triggers in the progression to heart failure and sudden death,” *Pflugers Arch. Eur. J. Physiol.*, vol. 466, no. 6, pp. 1189–1197, 2014, doi: 10.1007/S00424-014-1457-7.
[40] M. B. Bastos, D. Burkhoff, J. Maly, J. Daemen, C. A. Den Uil, K. Ameloot, M. Lenzen, F. Mahfoud, F. Zijlstra, J. J. Schreuder, and N. M. Van Mieghem, “Invasive left ventricle pressure-volume analysis: overview and practical clinical implications,” *Eur. Heart J.*, vol. 41, no. 12, pp. 1286–1297, Mar. 2020, doi: 10.1093/EURHEARTJ/EHZ552.
[41] J. I. Colorado-Cervantes, P. Nardinocchi, P. Piras, V. Sansalone, L. Teresi, C. Torromeo, and P. E. Puddu, “Patient-specific modeling of left ventricle mechanics,” *Acta Mech. Sin*, vol. 38, p. 621211, 2022, doi: 10.1007/s10409-021-09041-0.
[42] A. I. Hassaballah, M. A. Hassan, A. N. Mardi, and M. Hamdi, “An Inverse Finite Element Method for Determining the Tissue Compressibility of Human Left Ventricular Wall during the Cardiac Cycle,” *PLoS One*, vol. 8, no. 12, p. 82703, Dec. 2013, doi: 10.1371/JOURNAL.PONE.0082703.
[43] A. Heidari *et al.*, “Patient-specific finite element analysis of heart failure and the impact of surgical intervention in pulmonary hypertension secondary to mitral valve disease,” vol. 1, p. 3, 2022, doi: 10.1007/s11517-022-02556-6.
[44] “Abaqus 6.14 Documentation.” http://130.149.89.49:2080/v6.14/ (accessed Apr. 12, 2023).
[45] W. Gentzsch and F. Sahli, “Stanford Living Heart Project Focusing on Drug Induced Arrhythmia with Abaqus in the Cloud.”
[46] G. A. Brecher, H. Kolder, and A. D. Horres, “Ventricular Volume of Nonbeating Excised Dog Hearts in the State of Elastic Equilibrium,” *Circ. Res.*, vol. 19, no. 6, pp. 1080–1085, 1966, doi: 10.1161/01.RES.19.6.1080.
[47] J. V. Tyberg, W. J. Keon, E. H. Sonnenblick, and C. W. Urschel, “Mechanics of ventricular diastole,” *Cardiovasc. Res.*, vol. 4, no. 4, pp. 423–428, Oct. 1970, doi: 10.1093/CVR/4.4.423.
[48] M. Hori, E. L. Yeliin, and E. H. Sonnenblick, “Left ventricular diastolic suction as a mechanism of ventricular filling,” *Jpn. Circ. J.*, vol. 46, no. 1, pp. 124–129, 1982, doi: 10.1253/JCJ.46.124.
[49] S. Nikolic, E. L. Yellin, K. Tamura, H. Vetter, T. Tamura, J. S. Meisner, and R. W. M. Frater, “Passive Properties of Canine Left Ventricle: Diastolic Stiffness and Restoring Forces,” Accessed: Apr. 12, 2023. [Online]. Available: http://ahajournals.org.
[50] G. A. BRECHER, “Experimental evidence of ventricular diastolic suction,” *Circ. Res.*, vol. 4, no. 5, pp. 513–518, 1956, doi: 10.1161/01.RES.4.5.513.
[51] C. H. Park, W. H. Chow, and D. G. Gibson, “Phase differences between left ventricular wall motion and transmitral flow in man: evidence for involvement of ventricular restoring forces in normal rapid filling,” *Int. J. Cardiol.*, vol. 24, no. 3, pp. 347–354, Sep. 1989, doi: 10.1016/0167-5273(89)90014-4.
[52] H. Fukuta and W. C. Little, “The Cardiac Cycle and the Physiologic Basis of Left Ventricular Contraction, Ejection, Relaxation, and Filling,” *Heart Fail. Clin.*, vol. 4, no. 1, pp. 1–11, Jan. 2008, doi: 10.1016/J.HFC.2007.10.004.
[53] J. Concannon and J. P. McGarry, “Development of an FEA framework for analysis of subject-specific aortic compliance based on 4D flow MRI,” *Acta Biomater.*, vol. 125, pp. 154–171, Apr. 2021, doi: 10.1016/J.ACTBIO.2021.02.027.
[54] J. Concannon and J. P. McGarry, “Development of an FEA Framework for Analysis of Subject-Specific Aortic Compliance based on 4D Flow MRI,” *Acta Biomater.*, 2021.
[55] D. . Nolan, R. W. Ogden, M. Destrade, and J. P. McGarry, “A robust anisotropic hyperelastic formulation for the modelling of soft tissue,” *J. Mech. Behav. Biomed. Mater.*, 2014.
[56] J. P. McGarry, J. Fu, M. T. Yang, C. S. Chen, R. M. McMeeking, A. G. Evans, and V. S. Deshpande, “Simulation of the contractile response of cells on an array of micro-posts,” *Philos. Trans. R. Soc. A Math. Phys. Eng. Sci.*, vol. 367, no. 1902, pp. 3477–3497, Sep. 2009, doi: 10.1098/rsta.2009.0097.
[57] M. Ahmadian *et al.*, “A cross-species validation of single-beat metrics of cardiac contractility,” *J. Physiol.*, vol. 600, no. 22, pp. 4779–4806, Nov. 2022, doi: 10.1113/JP283319.
[58] S. Mohri, M. Dickstein, Y. Mika, J. Shimizu, I. Shemer, J. Wang, S. Ben-haim, D. Burkhoff,

K.-L. He, G.-H. Yi, and S. Ben-Haim, “Cardiac contractility modulation by electric currents applied during the refractory period,” 2002, doi: 10.1152/ajpheart.00959.2001.-Inotropic.

[59] A. J. Crottogini, P. Willshaw, J. G. Barra, and R. H. Pichel, “Left ventricular end-systolic elastance is incorrectly estimated by the use of stepwise afterload variations in conscious, unsedated, autonomically intact dogs,” *Circulation*, vol. 90, no. 3, pp. 1431–1440, 1994, doi: 10.1161/01.CIR.90.3.1431.

[60] A. Giudici, I. B. Wilkinson, and A. W. Khir, “Review of the Techniques Used for Investigating the Role Elastin and Collagen Play in Arterial Wall Mechanics,” *IEEE Rev. Biomed. Eng.*, vol. 14, pp. 256–269, 2021, doi: 10.1109/RBME.2020.3005448.

[61] A. Mookhoek, K. Krishnan, S. Chitsaz, H. Kuang, L. Ge, P. H. Schoof, A. J. J. C. Bogers, J. J. M. Takkenberg, and E. E. Tseng, “Biomechanics of Failed Pulmonary Autografts Compared to Native Aortic Roots,” *Ann. Thorac. Surg.*, vol. 103, no. 5, pp. 1482–1488, May 2017, doi: 10.1016/J.ATHORACSUR.2016.08.061.

[62] D. Zhalmuratova, T. G. La, K. T. T. Yu, A. R. A. Szojka, S. H. J. Andrews, A. B. Adesida, C. Il Kim, D. S. Nobes, D. H. Freed, and H. J. Chung, “Mimicking ‘j-Shaped’ and Anisotropic Stress-Strain Behavior of Human and Porcine Aorta by Fabric-Reinforced Elastomer Composites,” *ACS Appl. Mater. Interfaces*, vol. 11, no. 36, pp. 33323–33335, Sep. 2019, doi: 10.1021/ACSAMI.9B10524/SUPPL_FILE/AM9B10524_SI_001.PDF.

[63] J. Concannon, N. Hynes, M. McMullen, E. Smyth, K. Moerman, P. E. McHugh, S. Sultan, C. Karmonik, and J. P. McGarry, “A Dual-VENC Four-Dimensional Flow MRI Framework for Analysis of Subject-Specific Heterogeneous Nonlinear Vessel Deformation,” *J. Heat Transfer*, vol. 142, no. 11, Nov. 2020, doi: 10.1115/1.4048649/1087598.

[64] J. Concannon, K. Moerman, N. Hynes, S. Sultan, and J. McGarry, “Influence of shape-memory stent grafts on local aortic compliance,” *Biomech. Model. Mechanobiol.*, vol. 20, no. 6, pp. 2373–2392, Dec. 2021, doi: 10.1007/S10237-021-01514-9.

[65] C. V. Ioannou, D. R. Morel, A. N. Katsamouris, S. Katranitsa, I. Startchik, A. Kalangos, N. Westerhof, and N. Stergiopulos, “Left ventricular hypertrophy induced by reduced aortic compliance,” *J. Vasc. Res.*, vol. 46, no. 5, pp. 417–425, Aug. 2009, doi: 10.1159/000194272.

[66] R. Fagard and J. Staessen, “Relation of cardiac output at rest and during exercise to age in essential hypertension,” *Am. J. Cardiol.*, vol. 67, no. 7, pp. 585–589, Mar. 1991, doi: 10.1016/0002-9149(91)90896-S.

[67] A. Faragli, R. Tanacli, C. Kolp, D. Abawi, T. Lapinskas, C. Stehning, B. Schnackenburg, F. P. Lo Muzio, L. Fassina, B. Pieske, E. Nagel, H. Post, S. Kelle, and A. Alogna, “Cardiovascular magnetic resonance-derived left ventricular mechanics-strain, cardiac power and end-systolic elastance under various inotropic states in swine,” *J. Cardiovasc. Magn. Reson.*, vol. 22, no. 1, Dec. 2020, doi: 10.1186/S12968-020-00679-Z.

[68] Y. Zhang, J. Adams, V. Y. Wang, L. Horwitz, M. Tartibi, A. E. Morgan, J. Kim, A. W. Wallace, J. W. Weinsaft, L. Ge, and M. B. Ratcliffe, “A finite element model of the cardiac ventricles with coupled circulation: Biventricular mesh generation with hexahedral elements, airbags and a functional mockup interface to the circulation,” *Comput. Biol. Med.*, vol. 137, Oct. 2021, doi: 10.1016/J.COMPBIOMED.2021.104840.

[69] M. A. Habigt, M. Krieger, J. Gesenhues, M. Ketelhut, M. Mechelinck, and M. Hein, “Non-linearity of end-systolic pressure–volume relation in afterload increases is caused by an overlay of shortening deactivation and the Frank–Starling mechanism,” *Sci. Reports 2021 111*, vol. 11, no. 1, pp. 1–11, Feb. 2021, doi: 10.1038/s41598-021-82791-3.

[70] A. V. Delicce and A. N. Makaryus, “Physiology, Frank Starling Law,” *StatPearls*, Jan. 2023, Accessed: Apr. 13, 2023. [Online]. Available: https://www.ncbi.nlm.nih.gov/books/NBK470295/.

[71] M. Bloksgaard, T. M. Leurgans, B. Spronck, M. H. G. Heusinkveld, B. Thorsted, K. Rosenstand, I. Nissen, U. M. Hansen, J. R. Brewer, L. A. Bagatolli, L. M. Rasmussen, A. Irmukhamedov, K. D. Reesink, and J. G. R. De Mey, “Imaging and modeling of acute pressure-induced changes of collagen and elastin microarchitectures in pig and human resistance arteries,” *Am. J. Physiol. Heart Circ. Physiol.*, vol. 313, no. 1, pp. H164–H178, 2017, doi: 10.1152/AJPHEART.00110.2017.

[72] M. J. Chow, R. Turcotte, C. P. Lin, and Y. Zhang, “Arterial extracellular matrix: a

mechanobiological study of the contributions and interactions of elastin and collagen," *Biophys. J.*, vol. 106, no. 12, pp. 2684–2692, Jun. 2014, doi: 10.1016/J.BPJ.2014.05.014.

[73] T. M. J. Van Bakel, C. J. Arthurs, F. J. H. Nauta, K. A. Eagle, J. A. Van Herwaarden, F. L. Moll, S. Trimarchi, H. J. Patel, and C. A. Figueroa, "Cardiac remodelling following thoracic endovascular aortic repair for descending aortic aneurysms," *Eur. J. Cardiothorac. Surg.*, vol. 55, no. 6, p. 1061, Jun. 2019, doi: 10.1093/EJCTS/EZY399.

[74] S. Sultan, Y. Acharya, M. Hazima, H. Salahat, J. C. Parodi, and N. Hynes, "Combined thoracic endovascular aortic repair and endovascular aneurysm repair and the long-term consequences of altered cardiovascular haemodynamics on morbidity and mortality: case series and literature review," *Eur. Hear. journal. Case reports*, vol. 5, no. 10, Oct. 2021, doi: 10.1093/EHJCR/YTAB339.

[75] S. Sultan, J. Concannon, J. M. G. Patrick, P. E. McHugh, N. Barrett, and N. Hynes, "Early results and lessons learned using the streamliner multilayer flow modulator in the management of complex thoracoabdominal aortic aneurysms and chronic symptomatic aortic dissection," *Ital. J. Vasc. Endovasc. Surg.*, vol. 27, no. 3, pp. 146–156, Sep. 2020, doi: 10.23736/S1824-4777.20.01445-X.

[76] F. J. H. Nauta, H. W. L. de Beaufort, M. Conti, S. Marconi, A. V. Kamman, A. Ferrara, J. A. van Herwaarden, F. L. Moll, F. Auricchio, and S. Trimarchi, "Impact of thoracic endovascular aortic repair on radial strain in an ex vivo porcine model," *Eur. J. Cardio-Thoracic Surg.*, vol. 51, no. 4, pp. 783–789, Apr. 2017, doi: 10.1093/EJCTS/EZW393.

[77] T. OBrien, L. Morris, and T. McGloughlin, "Evidence suggests rigid aortic grafts increase systolic blood pressure: results of a preliminary study," *Med. Eng. Phys.*, vol. 30, no. 1, pp. 109–115, Jan. 2008, doi: 10.1016/J.MEDENGPHY.2007.01.004.

[78] Y. Yamashita, Y. Oishi, Y. Motomatsu, K. Hirayama, T. Harada, T. Ushijima, S. Fujita, S. Kimura, H. Sonoda, H. Tatewaki, Y. Tanoue, G. Sunagawa, T. Nishikawa, K. Saku, and A. Shiose, "Thoracic endografting increases cardiac afterload and leads to left ventricular hypertrophy in dogs," *Eur. J. Cardio-Thoracic Surg.*, vol. 55, no. 4, pp. 618–625, Apr. 2019, doi: 10.1093/EJCTS/EZY402.

[79] T. Murakami, "Enhanced Aortic Pressure Wave Reflection in Patients with Aortic Coarctation after Aortic Arch Repair," *Pulse*, vol. 5, no. 1–4, p. 82, 2018, doi: 10.1159/000478530.

[80] H. Alderson and M. Zamir, "Effects of stent stiffness on local haemodynamics with particular reference to wave reflections," *J. Biomech.*, vol. 37, no. 3, pp. 339–348, Mar. 2004, doi: 10.1016/S0021-9290(03)00289-6.

[81] C. V. Ioannou, N. Stergiopulos, A. N. Katsamouris, I. Startchik, A. Kalangos, M. J. Licker, N. Westerhof, and D. R. Morel, "Hemodynamics induced after acute reduction of proximal thoracic aorta compliance," *Eur. J. Vasc. Endovasc. Surg.*, vol. 26, no. 2, pp. 195–204, Aug. 2003, doi: 10.1053/ejvs.2002.1917.

[82] T. Takaseya and H. Aoki, "Endovascular Aneurysm Repair Increases Aortic Stiffness And Central Aortic Pressure," 2017. https://meetings.ismics.org/abstracts/2017/CMP17.cgi (accessed Apr. 13, 2023).

[83] R. P. Kelly, R. Tunin, and D. A. Kass, "Effect of Reduced Aortic Compliance on Cardiac Efficiency and Contractile Function of In Situ Canine Left Ventricle," Accessed: Apr. 13, 2023. [Online]. Available: http://ahajournals.org.

[84] M. Sarraf, D. Burkhoff, and M. I. Brener, "First-in-Man 4-Chamber Pressure–Volume Analysis During Transcatheter Aortic Valve Replacement for Bicuspid Aortic Valve Disease," *JACC Case Reports*, vol. 3, no. 1, pp. 77–81, Jan. 2021, doi: 10.1016/J.JACCAS.2020.11.041.